Juno Energetic Neutral Atom (ENA) Remote Measurements of Magnetospheric Injection-Dynamics in Jupiter's Io Torus Regions

B. H. Mauk[1], G. Clark[1], F. Allegrini[2,3], F. Bagenal[4], S. J. Bolton[2], J. E. P. Connerney[5,6], D. K. Haggerty[1], P. Kollmann[1], D. G. Mitchell[1], C. P. Paranicas[1], A. M. Rymer[1]

[1]The Johns Hopkins University Applied Physics Laboratory, Laurel, Maryland, USA (Barry.Mauk@jhuapl.edu)

[2]Southwest Research Institute, San Antonio, Texas, USA

[3]Physics and Astronomy Department, University of Texas at San Antonio, Texas, USA

[4]University of Colorado, Laboratory for Space and Atmospheric Sciences, Boulder, Colorado, USA

[5]NASA Goddard Space Flight Center, Greenbelt, Maryland, USA

[6]Space Research Corporation, Annapolis, Maryland, USA

Corresponding author: Barry H. Mauk (Barry.Mauk@jhuapl.edu)

Key Points:

- The first Jovian off-equator Energetic Neutral Atom (ENA) viewings reveal distinct emissions from Jupiter and the orbits of Io and Europa.
- Strong ENA emissions from Io's orbit are associated with energetic particle injections near Io's orbit observed several hours earlier.
- Energetic particle injections occur inside Io's orbit, a surprise given expectations that outward transport from Io drives injections.

Abstract

In planetary magnetospheres, singly charged energetic particles, trapped by the planet's magnetic field, can steal electrons from cold gas atoms and become neutralized. These now Energetic Neutral Atoms (ENAs), no longer confined by the magnetic field, can travel out of the system similar to photons leaving a hot oven. ENA's have been used to image magnetospheric processes at Earth, Jupiter, and Saturn. At Jupiter, the opportunities to image the magnetosphere have been limited and always from the perspective of the near-equatorial plane at distance >139 RJ. The polar orbiting Juno mission carries the JEDI instrument that is serendipitously sensitive to ENA's with energies > 50 keV, provided there are no charged particles in the environment to mask their presence. Here we report on the first ENA observations of Jupiter's magnetosphere from a non-equatorial perspective. In this brief report we concentrate on emissions seen during perijove 22 (PJ22) during very active conditions, and compare them with emissions during the inactive perijove 23 (PJ23). We observe, and discriminate between, distinct ENA signatures from the neutral gases occupying the orbit of Io (away from Io itself), the orbit of Europa (away from Europa), and from Jupiter itself. Strong ENA emissions from Io's orbit during PJ22 are associated with energetic particle injections observed near Io's orbit several hours earlier. Some injections occurred planetward of Io's L-shell (magnetic position), somewhat of a surprise given that injections are thought to be driven by outward transport of plasmas generated by Io.

Plain Language Summary

In the space environments of magnetized planets (magnetospheres), magnetic fields trap and confine energetic charged particles like protons and singly charged heavier ions. These ions can neutralize themselves by stealing electrons from cold gas atoms within the same environment. They become Energetic Neutral Atoms (ENAs), and no longer confined by the magnetic field, travel out of the system in a fashion similar to light leaving a hot oven. ENA's have been used to image magnetospheric processes at Earth, Jupiter, and Saturn. At Jupiter, the opportunities to image the magnetosphere have been limited and always from the perspective of the near-equatorial plane at large distances (>139 Jupiter radii). The polar orbiting Juno mission carries the Jupiter Energetic particle Detector Instrument (JEDI) that is serendipitously sensitive to ENA's with energies > 50 kilo-electron volts, provided there are no charged particles in the environment to mask their presence. Here we report on the first ENA observations of Jupiter's magnetosphere from a non-equatorial perspective. That perspective allows us to observe distinct ENA signatures from the neutral gases occupying the orbit of the moon Io (away from Io itself), the gases in the orbit of the moon Europa (away from Europa), and from Jupiter itself.

1 Introduction and Background

Energetic Neutral Atoms (ENAs) have been directly observed coming from the magnetosphere of Jupiter by Voyager (Kirch et al., 1981) and by the Cassini spacecraft as it flew by Jupiter on its way to Saturn (Krimigis et al., 2002; Mauk et al., 2003; 2004; Mitchell et al., 2004). Because of the spatial extent of the admittedly poorly imaged structures, Mauk et al. (2003, 2004) concluded that neutral gases in the orbit of Europa contributed greatly to the hydrogen ENA's observed with energies between 50 and 80 keV. The independent determination of the presence of substantial neutral gases in Europa's orbit by Lagg et al. (2003) and Kollmann et al., 2016), and the recent evaluation of the role of neutral gases relative to plasmas by Smith et al. (2019), give additional confidence to this conclusion. Mitchell et al (2004) showed that both neutral hydrogen (H) and neutral heavy atoms (presumably O and S) were emitted by the

magnetosphere. These authors showed that the emissions varied very little over an 80 day period. Plainaki et al. (2018) provided additional reconstruction of the Cassini-observed ENA emissions from Jupiter and showed substantial azimuthal (around Jupiter) asymmetry in the emissions. Roelof (1987) initiated the concept of using ENAs to image magnetospheric structures.

These previous ENA observations of Jupiter were made under conditions that were quite limiting. The equatorial perspective led to ambiguity in identification of the source, since emissions from Io's orbit or from Jupiter itself had to be viewed through Europa's environment. While Mauk et al. (2003, 2004) concluded that an observed central structure represented emissions from Jupiter itself (that is, from Jupiter's exosphere interacting with nearly precipitating ions), that conclusion has been challenged in subsequent informal discussions given the possibility that that structure came from non-uniform gas distributions around Europa's orbit. The ENA emission studies performed subsequently at Saturn, with a highly capable ENA camera situated at ideal positions relative to the Saturnian system, made it clear how valuable ENA studies can be for characterizing the dynamics of a magnetosphere (Mitchell et al., 2005; 2009a, 2009b).

The Juno spacecraft, now in a polar orbit around Jupiter, does not carry an instrument designed to measure ENA's. However, its energetic particle instrument, the Jupiter Energetic particle Detector Instrument (JEDI) can measure ENA's with energies > 50 keV provided there are no charged particles around to mask the presence of the ENA's. We report here that JEDI does indeed observe ENA's coming from Jupiter's inner magnetosphere. Juno obtains these observations from high Jovigraphic latitudes when the spacecraft is on magnetic field lines that connect to Jupiter's polar cap, where the energetic charged particle populations are very sparse. Several different ENA components are observed as reported here, but the most unique measurements are of the Io plasma torus regions, emissions that are tied here directly to the dynamical state of the Io orbital regions.

In the sections that follow, we discuss the Juno and the JEDI measurement capabilities, analyze the observed ENA emissions, we discuss the relationship between the ENA measurements and in situ measurements within the remotely sensed regions, and we conclude with a discussion and summary.

2 Juno and JEDI configurations.

The Juno mission was launched in 2011, and was inserted into Jupiter orbit in July of 2016 with the following characteristics: 1.05 x 112 RJ polar (~90° inclination), ~53.5 day period elliptical orbit with the line-of-apsides close to the dawn equatorial meridian. Following insertion, the line-of-apsides has been slowly precessing southward (~ 1° per orbit) and towards the night-side (~4° per orbit). Juno targets multiple disciplines including Jupiter's interior, atmosphere, polar space environment and its powerful aurora (Bolton et al.; 2017a; Bagenal et al., 2017). Bolton et al. (2017b) and Connerney et al. (2017a) presented initial findings for all disciplines.

We focus in this study on measurements from the Jupiter Energetic-particle Detector Instrument (JEDI; Mauk et al., 2017). JEDI was designed to measures energy, angular, and compositional distributions of electrons (~ 25 to ~1200 keV) and ions (protons: ~10 keV to > 1.5 MeV; oxygen and sulfur from ~145 keV to > 10 MeV)). It uses solid state detectors (SSDs), thin

foils, and Microchannel Plate detectors (MCPs) to measure electron SSD singles rates (SSDs shielded by 2μ Al), time-of-flight by energy (TOFxE) for higher energy ions, and time-of-flight by MCP pulse height (TOFxPH) for lower energy ions. It is critical to note that JEDI measures atoms whether or not they are charged. The first material interaction that a particle makes with the JEDI instrument is the penetration of a very thin foil within the collimator. That foil redistributes the charge state of the particle, and so the initial charge state of the particle is lost in any case. Mauk et al. (2020) provides an overview of the findings of the JEDI investigation over Jupiter's polar-regions.

JEDI is a complement to the lower energy Jupiter Auroral Distributions Experiment (JADE) instrument. JADE measures distributions of electrons from 100 eV to 100 keV, and of ions with composition up to 46 keV/q, where q is electric charge (McComas et al., 2017). Allegrini et al., 2017 and Szalay et al., 2017 published initial results from JADE over Jupiter's polar regions. However, unlike JEDI, JADE does not detect neutral atoms because electrostatic deflection is a critical aspect of the JADE measurements.

JEDI consists of 3 independent instruments, each of which has 6 telescopes arranged in a ~160° fan. Figure 1b shows the configuration of these three instruments (JEDI-90 or J90, J180, and J270). J90 and J270 are oriented to approximate a 360° field of view within a plane roughly perpendicular to the spacecraft spin vector. Only J90 and J270 measure ions and ENA's; J180 is configured to measure only electrons because of a problem with its high voltage operation. The 160° fans of J90 and J270 do not reside exactly perpendicular to the spin axis; their orientations are tilted and twisted by up to 10° to avoid viewing the huge Juno solar panels. The full-width at half maximum angle (FWHM) resolution of JEDI is roughly 17°x 9°, with the 17° dimension oriented along the 160° fan. In high-resolution mode, JEDI accumulates for 0.25 seconds at a cadence of 0.5 seconds (ions and electron measurements are sub-commutated). Hence, given the 30s spin period of Juno, the field-of-view is rotated by 3° during an accumulation. The 17° opening for the telescopes is obviously much wider than one would want in an imaging instrument. However, the locations of narrow features can be determined much more accurately by centroiding the sensor response as the spacecraft spins around at a 30-second cadence. The 12 different telescopes oversample the structure by cutting through it with different rotational phasing with respect to the structure as the sensors accumulates over 3° intervals every 6°. An important element in determining whether JEDI is measuring charged particles or ENAs is an examination of how ordered or disordered the particle angular distributions are with respect to the local magnetic field. Hence, the magnetometer measurements on Juno (MAG; Connerney et al., 2017b) are critical to the ENA sensing reported here.

Figure 1a shows the particular Juno orbit that will be the focus of this paper. Here the perspective is from infinity along the dawn axis. For this particular time frame, the orbit resides roughly within the noon-midnight meridian. The observations that we will highlight are those made at the positions on Juno's orbit shown with purple bulges (the first and last of which are labeled with the times 0512 and 0815). At those times, Juno does not reside within the intense charge particle environments of Jupiter. It resides, rather, on magnetic field lines that connect to Jupiter's polar cap, where the charged particle populations are often very sparse. The spin axis of Juno points roughly towards the sun (towards Earth to be more precise), and the JEDI ion and ENA measurement all take place roughly (although not exactly) within a plane that is

perpendicular to the sun line. In essence, JEDI obtains a 1-dimensional, 360° image in a direction roughly normal to the sun line.

3 JEDI ENA Measurements

Figure 2 shows selected JEDI measurements along the trajectory shown in Figure 1a. The data shown are JEDI measurements of the combined Oxygen (O) and Sulfur (S) channels (> 144 keV). The top panel is a standard survey pitch-angle versus intensity distribution plot, with 30s time averaging. Here, pitch angle is the angle between the local magnetic field direction and the velocity vector of the particles that are measured. Prior to about the time of 0450, Juno is within the "Charge Particle Domain" identified schematically in Figure 1a. After that time, Juno enters the Polar Cap Domain. Even though the charged particles are sparse within the Polar Cap Domain, there are distinctive and repeatable charged particle signatures. Specifically, in the top panel, there is a feature labeled "ions" which corresponds to O and S ions accelerated downward onto the atmosphere by magnetic field-aligned electric potentials that are at the megavolt level (Clark et al., 2018; Mauk et al. 2020). However, the speckled feature within this top panel, labeled "ENAs", is clearly not a charged particle feature. If this feature is attributed to charged particles, it would correspond to O and S ions with hundreds of keV coming up from Jupiter's low altitude regions in the absence of a substantial down-going component. Additionally, this feature shows no perturbation as it crosses the time of the ion feature mentioned above. Given that that ion feature corresponds to megavolts of downward electrostatic potential above the spacecraft, there is no way that one could observe up-going ions of several hundred keV without seeing the downward reflection of those ions. The broader feature to the right (labeled "?") may have had charged particles mixed in with the ENA feature.

Once one concludes that the particles are neutral, pitch angle ordering is no longer appropriate. The second panel of Figure 2 is an "Azimuth" versus intensity distribution plot with 300 second averaging. Azimuth is an angle within the JSO-Y and JSO-Z plane, defined in Figure 1b. Here we see some very distinctive features, labeled in the left side of the panel. The lowest feature is the ion feature that was also labeled ions in the top panel. However, three other features have emerged, labeled "Feature A", "Feature B" and "Feature C". Feature B does not really resolve itself until we do more averaging. In the third panel, we average over 600 seconds (10 minutes) and change over from a color scale showing intensity to one showing counts-per-bin. Here the resolution of Feature C is becoming a little clearer. A detailed, digital and formal examination of the counts corresponding to these features shows that there is a very consistent count minimum between Feature A and B. Figure 3a shows the results of that formal examination. Here we have generated running centroid positions for the three features. This examination uses 10-minute averages at a cadence of 5 minutes. We will return to Figure 3 in Section 4.

The bottom panel of Figure 2 shows the energy distribution for the "mostly ENA" features. For this panel we extracted the energy distributions from the data in the top panel by selecting only pitch angles greater than 110°. Because this averaging process includes a lot of the empty space between the features of interest (given limitations in our software), we renormalized the labels on the color scale by a factor of 10 to yield the approximate peak intensity for the lowest energy channel for Feature A. We see finite intensities up to several MeV. We assume that the ENAs result from charge exchange interactions between heavy ions (O^+ and S^+) and heavy neutral gases (O and S; we discuss in Section 7 the possiblility that cold

ions in additions to cold neutrals are involved). Figure S1 in the Supporting Information section repeats a charge exchange cross section plot published by McEntire and Mitchell (1989). We see there that for O+ interacting with O, finite interactions occur at energies as high as several MeV, qualitatively consistent with our observations.

Figure 4 shows a plot similar to Figure 2 but for > 50 keV hydrogen. While the strongest ENA features previously identified are still in evidence, there appears to be a greater amount of charged H^+ particle contamination of the hydrogen ENA measurements. We will say little more about the hydrogen ENAs in this first publication.

4 JEDI ENA Viewing Analysis

The scatter plots in Figure 3a represent the average or centroid of the azimuth locations of each of the three features identified at each time (5-minute cadences are used with 10-minute averaging). The scatter within each feature is a reflection of the counting statistics uncertainties engendered by the very low number of counts within each bin. Feature A has a lower amount of scattering because the counts per bin are higher. To average out the scattering we have generated analytic fits to each of the features, as shown on the figure. The fits are derived by choosing an appropriate analytic functional form and then optimizing the free parameters of those functional forms by minimizing the sum of the squared differences between the data and the function (i. e., a chi^2 type procedure). The fits are as follows:

$$\text{A:Azimuth}(^\circ) = 36.93\ (\text{Tanh}[0.667\ (\text{TH} - 4.679)])^{0.5058} \quad (1)$$

$$\text{B:Azimuth}(^\circ) = -1.9038\ (\text{TH}^2) + 20.79\ \text{TH} + 19.166 \quad (2)$$

$$\text{C:Azimuth}(^\circ) = -1.6588\ (\text{TH}^2) + 14.275\ \text{TH} + 130.38 \quad (3)$$

Here TH is the time in hours for Day 255, 2019. These fits are used to evaluate the look directions of JEDI within the context of the Jovian system. Figure 5 shows the results of that analysis. The figure shows the look directions associated with Feature A with green lines starting from the Juno orbital position at each of several different times along the trajectory. It shows the look directions of Feature B and C with grey and dashed-blue lines, respectively.

We conclude that the strongest Feature A is associated with emissions from the vicinity of Io's orbit. The relatively weaker Features B and C appear to be coming, respectively, from Jupiter itself and from the orbit of Europa (or slightly inside of the orbit of Europa). With regard to the emissions coming from the orbits of Io and Europa, one must recognized that the energetic particle populations might be just as intense, or indeed more intense, between the two orbits, or otherwise away from the two orbits. The orbital positions of Io and Europa are favored for the emissions because the neutral gas populations (and cold ion populations) maximize at just those orbits (Smyth and Marconi, 2006). Figure 6 shows what kinds of shifts in the fits one would need to alter the interpretations. For Feature A at the bottom of the figure, the shift shown would move the fields of view from the Io orbit to the Europa orbit. For Feature B at the middle, the shift shown would move the fields of view by1 RJ at Jupiter with respect to where they are now. For Feature C, the shift shown would move the fields of view from the Europa orbit to the Io orbit. Feature A and C are well constrained. The most uncertainty is with Feature B.

The analysis shown in Figure 6 is strictly geometric based on the centroids of the observed ENA features. For that analysis there is no consideration of the nature of the environment from which the ENA's are coming. The apparent strong focusing of the green lines just on the orbit of Io may mislead some viewers. One expects that the cloud of neutrals and possibly cold plasmas that serve to convert the trapped ions into ENA's have vertical and radial extents that may be as large as ±1 RJ (e. g. Bagenal et al., 2020). It is likely that the ENAs are coming from an extended region around the Io orbit that reflects the distribution of these components. If JEDI were reading thousands of counts per accumulation rather than just 10-20, we could contemplate deconvolving the measurements from the distribution of emitters (using, for example, a forward-model inversion process) to reveal the spatial structure of the emitting regions. Given the limitations of the counts available, the best that we can do right now is to determine the centroid of the emitting region. Given present knowledge about the emitting regions, the fact that the centroid focuses so closely on the orbit of Io means that the spatially extended emitting region must be roughly symmetric around that position.

Figure 7 shows other aspects of the JEDI viewing associated with the ENA emissions. Figure 7a confirms that Feature B is associated with views that roughly intersect Jupiter itself. Figure 7a shows the grey lines tilted (by 5°) because the JEDI sensors do not precisely view perpendicular to the Juno spin axis. Around each of these centroid lines is a range of angles that extends perhaps as much as 10° on either side, given the peculiar twists to the offsets. A more accurate determination of just where and if these views encounter the planet must await the development of new tools and future studies.

We expect that ENA emissions from Jupiter itself will be very complicated. Most such ENAs are generated roughly normal to the magnetic field lines within the upper atmosphere at certain positions where ions are nearly precipitating and locally mirroring within the exosphere. Because we are examining heavy ions from the magnetosphere rather than light ions from the atmosphere, it is most likely that these ENA's coming from Jupiter are not the result of ions locally accelerated by auroral processes as observed at Saturn (Mitchell et al., 2009a). Because of the angle with which the magnetic field encounters the exosphere, there will be ions emitted with a substantial polar components to their velocities. All of these considerations of Jupiter as a source of ENA emissions must await future studies. For now, all we can say is that the viewing analysis makes it likely that Feature B is a consequence of ENAs coming from the close vicinity of Jupiter.

Figure 7b shows that the ENA emissions associated with Io and Europa do not come from the vicinity of Io or Europa themselves. They truly are associated with charge exchange interactions occurring with gases distributed along the orbits of these moons and not with gases close to the moons themselves.

It is finally of interest that the emissions from the orbit of Io and Europa are asymmetric. The emissions do not come uniformly around the orbit of these moons. The Io emissions are observed only on one side, and the Euorpa emissions are observed only on the other side. While it is expected that there are azimuth asymmetries in the neutral gas populations (e. g. Smyth and Marconi, 2006; Smith et al., 2019), we suggest that the emission asymmetries are probably dominated by azimuthal asymmetries in the energetic particle populations, given that those populations are transported by azimuthally constrained dynamic injections.

5 ENA Emission Variability

One test of the role of dynamic injections in the generation of asymmetries in the ENA emissions is an examination of the time variability of the emissions. Figure 3b examines short-time variations. This panel shows the total counts associated with each component of the emissions. The error bars are the ±1-standard-deviation error ($N^{1/2}$) based on the average counts within each component. For the Io component (A) there are hints of structure, but the maximum contrast at most local ups-and-downs corresponds to only two standard deviations. And so for the Io emissions, our data does not have the fidelity to identify local structures clearly. We do see significant variations for both the Jupiter component (B) and the Europa component (C). We believe that the variations in Feature C are likely associated with injection-induced variability in Europa's orbit. The causes of the quasi-periodic variations in the Jupiter (Feature B) component is unknown. Is this structure a temporal variation of a localized emission hot spot, or is it the result of spatial structure viewed as the instrument scans across the planet? There are also variations in the azimuth centroid positions (Figure 3A), but analyses show that they have no distinct correlation with the total counts variations (Figure 3B). This issue may possibly be resolvable once we create proper tools for displaying the data in the Jupiter context.

Longer-term temporal dynamics are observable by examining orbit-to-orbit variations. Once we recognized the ENA emissions in Perijove 22 (PJ22) survey plots, an examination of other perijoves revealed that ENA emissions are present in the JEDI data for essentially all of the perijoves. But, the intensities of the ENA emissions and the patterns of emission are quite variable. For this first study, we compare the ENAs from PJ22 with those of just one other perijove, PJ23. The value of using this particular perijove is that the orbital configuration is very similar to that of P22. The data from PJ23 for oxygen and sulfur is shown in Figure 8 with exactly the same plot parameters as those used for PJ22 in Figure 2. A casual glance at these two figures shows that the PJ23 emissions were substantially less intense than were the PJ22 emissions; the spatial configuration also seems very different.

In the next section, we address whether the variability in ENA emissions that we see between PJ22 and PJ23 makes sense from the perspective of the local environments of Io and Europa.

6 In-Situ Characterization

A valuable aspect of the Juno observations of ENA emissions on the outbound legs of the trajectories is that the spacecraft passes through the remotely sensed environments on the inbound legs just several hours before. Figures 9 and 10 show the data taken by JEDI in the vicinity of the Io and Europa orbits during those inbound time frames. While there is much to discuss here, one immediate conclusion is that the environment near Io's orbit is comparatively intense and dynamic during PJ22 (Figure 8) and relatively quiescent during PJ23 (Figure 9). This immediate observation is consistent with the fact that relatively intense ENA emissions occurred during PJ22 and not during PJ23.

6.1 JEDI measurements in Jupiter's hard radiation regions

Before discussing the implications of Figures 9 and 10 more completely, we provide here more details about their contents. From top to bottom these figure show the following: (a) intensities from one or more of our Oxygen and Sulfur channels (note that below about 600 keV,

JEDI cannot discriminate between O and S); (b) proton intensities in the form of Energy-Time-Intensity spectrograms; (c) the corresponding electron intensities with the energy scale inverted (helpful when studying injection phenomena); and (d) singles rates from the small pixel ion SSDs from JEDI-A180.

JEDI was not designed to make measurement within this region containing Jupiter's more intense radiation belts. The radiation belt electrons can compromise the electron measurements in particular. JEDI contains a feature to diagnose this condition. JEDI-A180 has two of its small-pixel ion SSD's covered with thin shields of titanium, and with 3 sister SSD's uncovered or bare (a 6th telescope is partially obscured by a sun shield). Absent any radiation that penetrates the side shielding of the instrument, the unshielded detectors measure electrons with energies > 25 keV, while the shielded detectors measure electrons with energies > 500 keV. When side-penetrating radiation belt electrons dominate, the response of all of these detectors become essentially the same. On the left portions of both Figures 9 and 10 we see that the unshielded detectors are reading higher values than are the shielded detectors, indicating that a good measurement of the foreground electron population is being made. On the right sides of both figures, the responses pinch together indicating that side-penetrating electrons are dominating the responses.

The ion measurements are much cleaner because they depend on coincidences between three different signals, a start pulse generated by the penetration of a thin start foil by the ion, a corresponding stop pulse, and a SSD pulse. None-the-less, intense electron radiation can compromise the ion measurements. The most vulnerable channels are those for heavy ions at the lowest energies because their times-of-flight are the longest. Electrons can generate what are termed "accidental" events. The red-dashed curves in the top panels of Figures 9 and 10 represent the estimated accidental rates corresponding to the lowest energy O+S channel (145-209 keV). We see that for PJ22 (Figure 9) the ion measurements are clean, whereas for PJ23 (Figure 10) there is a region just inside of Io's L-shell where the response of this channel is dominated by electrons. There are also features within the protons spectrogram of Figure 10 (labeled "e-") that show evidence of electron contamination.

6.2 Implications of the JEDI in-situ measurements

The ENAs for PJ22 in Figure 2 are not coming from the same populations as those shown for PJ22 in Figure 9. Figure 7b shows approximately, where on Io's orbit Juno crossed Io's L-shell. That crossing occurred between 3.5 and 6 hours prior to the time of the ENA measurements. Given that transport is dominated by rigid Jovian rotation (with only small deviations coming from magnetic drifts), the particles observed by Juno on the inbound would be rotated to 12-hour-clock positions between about 2 and 5 o'clock at the times of the ENA measurements. These positions were not within the field of view of JEDI. And, given that the ENA emissions themselves suggest that there are substantial azimuthal asymmetries, we cannot be assured that the in situ measurements are truly characterizing the populations that are being observed remotely.

But, what we can say is that during PJ22 (Figure 9), dynamic injections had recently populated the regions near and even inside Io's orbit (R = 5.9 RJ). Dynamic injections have been characterized in more distant regions by Mauk et al. (1999) and in regions as planetward as L=7 using Juno by Haggerty et al. (2019). One small-scale injection event studied by Thorne et al. (1997), and labeled an "interchange event," occurred just outside of Io's orbit, at about L =

6.02. And the auroral manifestations of such injections have been studied by Mauk et al. (2002) and Dumont et al., (2014), with the latter authors also finding injections as planetward as L = 7. Juno detected time-dispersed injections right at Io's L-shell in Figure 9 in both the H+ distributions and the O+S distributions. That these are time-dispersed features and not spatially dispersed features is evident from the fact that, for the H+ observations, the dispersion sense is the same when we cross inbound across Io's orbit and when we cross outbound. And, for PJ23 in Figure 10, we can say that there was no evidence of recent injection phenomena in the vicinity of Io's orbit. In fact, during PJ23, the regions near Io had been emptied substantially, presumably by persistent charge exchange interactions with the resident neutral gases. It is interesting, however, that there is evidence of recent injection phenomena during the PJ23 time frame further out, in the vicinity of Europa's orbit.

The system can generate ENAs emissions even in the absence of recent dynamic injections. Even in relatively quiet-times there is often a "ledge" of ion intensities just outside of Io's L-shell that can interact with the iogenic gases and generate ENA's. That ledge is evident in observations reported by Kollmann et al. (2017) and Paranicas et al. (2019), and is apparent in Figure 10 (top) in the O+S ions just outside of Io's L-shell. Over time, one expects that injections (thought to be the primary inward transport mechanisms for energetic particles) will populate the inner regions, and that iogenic gases and the moon itself will sculpt the resulting distributions into the distribution observed during quieter times. For the PJ22 case, we believe that recent dynamic injections play a key role in the heightened intensity of the ENA's observed during that time frame.

It is of interest to evaluate whether or not the intensities and neutral gasses within the Io regions are sufficient to account for the observed ENA intensities (Figure 2, bottom). To perform this calculation we use the following parameters. The O+S 144-209 keV channel intensity close to Io from Figure 9 is ($J(OS^+) \sim 3 \times 10^3$ 1/(cm^2.s.sr.keV)). We combine that parameter with an Io neutral torus density of N = 35/cm^2, a charge exchange cross section of $\sigma = 7 \times 10^{-16}$ cm^2 (Figure S1 in Supporting Information), and a neutral gas cloud thickness of s = 1-2 RJ (Io torus parameters reviewed by Bagenal et al., 2020). One finds with $J(ENA) = \int(\sigma N J(OS^+) ds$, that J(ENA) is expected to be about 0.5 to 1/(cm^2.s.sr.keV). And indeed, that value is within a factor of 2 of what we find for the lowest energy channel in the bottom panel of Figure 2. However, we acknowledge great uncertainty in the parameters used for these calculations.

One of the uncertainties in such calculations for Io is the possible role of cold plasma, in addition to cold neutral gases, in providing the neutralizing electrons for the energetic particles. Smith et al. (2019) showed for the Europa regions that cold ions can contribute to the neutralizing process even while neutral gases likely dominate. In Io's environment, the ratio of charged ions to neutral gases is much larger than it is for Europa (Bagenal et al., 2020). Hence, it may turn out to be true that charged ions, rather than neutral gases, play a dominant role in the neutralization process. This uncertainty needs to be investigated.

6.3 Miscellanea

An interesting question is: why we do not see more substantial O+S ENA emissions from the Europa region during the PJ23 time frame, given that the O+S ion intensities are relatively high near Europa. We remind ourselves that Juno inbound is not looking at the same populations that are remotely sensed during Juno outbound. However, one other possible answer resides

with the charge state of these ions. In their examination of the consequences of neutral gas in the vicinity of Europa on pitch angle distributions, Lagg et al. (2003) concluded that the heavy ions were multiply charged in the vicinity of Europa. Multiply charged heavy ions do not yield ENA emissions on interacting with neutral gas. As these ions are transported through the Europa regions and towards Io, the interactions with the neutral gases are thought to redistribute the charge states of these heavy ions, causing them to migrate towards singly charged states. More recently, Nénon and André (2019) showed evidence that the transition to singly charge states for heavy ions becomes significant just inside of Europa, as soon as 9.2 RJ as compared to the Europa position of 9.6 RJ. This finding is interesting given that the present observations of O+S ENA's from the Europa region seem to occur slightly inside of Europa's orbit (Figure 5; although we do not trust the viewing accuracy to this level of detail). Clark et al. (2016), in their diagnosis of charge states using time dispersion from dynamic injections, also found multiply charged heavy ions (O and S) outside of Europa, but sometimes singly charged populations were observed, suggesting that the results can change over time. And more recently, Clark et al. (2020; this issue) found that heavy ions from the most distant portions of Jupiter's magnetosphere (measured over Jupiter's polar cap) have mostly singly charge O and doubly charged S. Much more work using many more Juno orbits will be required before we can hope to obtain a convergence between the in situ and remote sensing observations.

One interesting sidelight to the injections observed near Io is that they extend inside of Io's L-shell. Here, in Figures 9 and 10, Io's L-shell is determined not using the magnetic field models, but by the local minima within the electron populations (bottom panels; however these locations are consistent with the field models). Because of the tilt of Jupiter's magnetic axis, a satellite like Io traverses a range of L-values as Jupiter rotates ($dL/L \sim \pm 1.5\%$ for a pure dipole). The local minima in the energetic electron population provides a mean value. It is somewhat of a surprise that such clear injections occur inside of Io's L-shell since outward transport of plasmas generated from Io are thought to drive the injection phenomena. Part of that surprise comes from comparisons with the work on the auroral manifestations of the injections by Dumont et al., (2014). These authors found no injection signatures at or inside of Io's L-positions. While we do not know why we are seeing such injections and Dumont et al. (2014) did not, we do know that injections observed in situ do not necessarily show up in auroral images (Haggerty et al., 2019). Also, there may be something about the innermost environment that suppresses such auroral manifestations. For example, the Io regions may have the wrong plasma environment for growing the waves that scatter the electrons into the loss cone. Paranicas et al. (2019) reported similar features as we now report inside Io's orbit, and identified them as transient populations.

It may be of interest that electron injections were not observed in association with the near-Io ion injections close to Io. Unfortunately the JEDI electron responses inside of Io' orbit were dominated by electrons with > 10-15 MeV energies that penetrated the sidewalls of the instrument. Modest electron injection signatures would not have been observed, however strong ones might have been. Past experience (e.g. Mauk et al., 1999) shows that injections are not always visible in both ions and electrons. That earlier work concluded that the visibility of an injection signature was a function of the radial (L) gradient in the phase space density (for constant adiabatic invariants). This conclusion was based on the deduction that injections represent relatively sudden planetward displacements of populations over limited azimuthal extents. Injections are invisible when the radial gradient is small, even when the radial

displacements are large. More events must be examined, and more work performed, before we know the reasons for the differences between electron and ion responses near Io.

7 Summary

In this first brief report, we aspire to introduce the capability of Juno to make ENA observations, and to report on the first such observations at Jupiter from a non-equatorial perspective. By doing so we have made the first definitive observation of ENA's with greater 10's of keV energy coming from the Io torus regions. We will perform evaluations that are more comprehensive once we develop proper tools in the months to come for projecting the ENA emissions onto the Jovian geometric system. These observations and analyses are particularly relevant to the European Space Agency JUICE mission to orbit Jupiter mission, with a planned arrival data of 2029, which will carry proper ENA imagers (Brandt et al., 2018; Futaana et al., 2015).

To summarize our findings:

1) The first non-equatorial observations of ENA emissions from Jupiter have revealed distinct and distinguishable emissions coming from the orbit of Io, the orbit of Europa, and from Jupiter itself. No previous observation has reported ENA emissions uniquely identified with Io with energies 10's to 100's of keV, even to several MeV.
2) The emissions from the orbits of Io and Europa are azimuthally asymmetric. Specifically for the particular PJ22 orbit examined, Io orbit emissions were observed distinctly only on the dusk side, and Europa orbit emissions were observed distinctly only on the dawn side. For at least the Europa emissions, time variability of the emissions over several hours reveal smaller scale azimuthal structure.
3) ENA emissions are clearly coming from the direction of Jupiter itself, but the tools available now are too crude to determine the region and mechanisms of emission. The likely cause is the simple precipitation of ions.
4) In situ measurements made near the orbits of Io and Europa several hours in advance of the ENA emissions, observed during PJ22, showed clear evidence of dynamic energetic particle injections right in the Io regions, and substantial O+S ion intensities, consistent with seeing relatively intense ENA emissions during that perijove. No such injections, and relatively low O+S intensities, were observed during PJ23, for which the ENA intensities were much lower.
5) Dynamic injections were observed inside of Io's L-shell, a modest surprise given that transport of plasmas outward from Io are thought to drive injections.

Acknowledgments and Data

We are grateful to NASA and contributing institutions that played critical roles in making the Juno mission possible, and particularly those numerous individuals at The Johns Hopkins University Applied Physics Laboratory (JHU/APL) who developed the JEDI instrument. We are grateful for Lead Engineer Charles E Schlemm and David B. LaVallee for their continued support of JEDI operations. We are grateful to JHU/APL's Lawrence E. Brown and James M. Peachey for their roles in developing and maintaining the data flow and display software used here. NASA's New Frontiers Program funded this work for Juno via subcontract with the Southwest Research Institute. The data presented here are available from the Planetary Plasma Interactions Node of NASA's Planetary Data System (https://pds-ppi.igpp.ucla.edu/). Also, ASCII dumps with header documentation has been performed for each panel of the JEDI data

displayed in this paper and is accessible at Zenodo (this submission is in process). The JEDI display software used here is available online and can be accessed by contacting the lead author. A one-hour teleconference tutorial provided by the lead author or his designate is generally sufficient for a user to have sufficient expertise to proceed.

References

Allegrini, F. et al. (2017), Electron beams and loss cones in the auroral regions of Jupiter. *Geophys. Res. Lett.*, 44, doi:10.1002/2017GL073180.

Bagenal, F., Adriani, A., Allegrini, F. et al. (2017), Magnetospheric Science Objectives of the Juno Mission. *Space Sci Rev*, 213, Iss. 1-4, pp 219-287, doi:10.1007/s11214-014-0036-8.

Bagenal, F., & Dols, V. (2020). The Space Environment of Io and Europa. *Journal of Geophysical Research: Space Physics*, 125, e2019JA027485. https://doi.org/10.1029/2019JA027485. .

Bolton et al. (2017a), The Juno mission. *Space Sci. Rev.*, 213, Iss. 1-4, pp 5-37, doi:org/10.1007/s11214-017-0429-6

Bolton, J. S. et al. (2017b), Jupiter's interior and deep atmosphere: The initial pole-to-pole passes with the Juno spacecraft. *Science*, 356, 6340, 821-825.

Brandt, P. C., S. Y. Hsieh, R. DeMajistre, and D. G. Mitchell, ENA imaging of planetary ring currents, in *Electric Currents in Geospace and Beyond*, edited by A. Keiling, O. Marghitu, and M. Wheatland, *Geophysical Monograph 235*, Chapter 9, pp 139-154, American Geophysical Union, Washington DC, doi:10.1002/9781119324522.

Clark, G., B. H. Mauk, C. Paranicas, P. Kollmann, and H. T. Smith (2016), Charge states of energetic oxygen and sulfur ions in Jupiter's magnetosphere. *J. Geophys. Res., Space Physics*, 121, 2264–2273, doi: 10.1002/2015JA022257.

Clark, G., et al. (2017a), Energetic particle signatures of magnetic field-aligned potentials over Jupiter's polar regions. *Geophys. Res. Lett.*, 44, 8703–8711, doi:10.1002/2017GL074366.

Connerney, JEP, et al. (2017a), Jupiter's magnetosphere and aurorae observed by the Juno spacecraft during its first polar orbits. *Science*, 356, 6340, 826-832, doi:10.1126/science.aam5928.

Connerney, J.E.P., Benn, M., Bjarno, J.B. et al. (2017b), The Juno magnetic field investigation. *Space Sci Rev.*, 213, Iss. 104, pp 39-138, doi:10.1007/s11214-017-0334-z (2017).

Connerney, J. E. P., Kotsiaros, S., Oliversen, R. J., Espley, J. R., Joergensen, J. L., Joergensen, P. S., et al. (2018). A new model of Jupiter's magnetic field from Juno's first nine orbits. *Geophys. Res. Lett.*, 45, 2590– 2596. https://doi.org/10.1002/2018GL077312.

Dumont, M., D. Grodent, A. Radioti, B. Bonfond, and J.-C. Gérard (2015), Jupiter's equatorward auroral features: Possible signatures of magnetospheric injections, J. Geophys. Res. Space Physics, 119, pages 10,068– 10,077. doi:10.1002/2014JA020527.

Futaana, Y., Barabash, S., Wang, X.-D., Wieser. M., Wieser, G. S., Wurz, P., Krupp, N., Brandt, P. (2015), Low-energy energetic neutral atom imaging of Io plasma and neutral tori, Planetary and Space Science, Volume 108, Pages 41-53, doi.org/10.1016/j.pss.2014.12.022.

Haggerty, D. K., Mauk, B. H., Paranicas, C. P., Clark, G., Kollmann, P., Rymer, A. M., et al. (2019). Jovian injections observed at high latitude. Geophysical Research Letters, 46, 9397–9404. https://doi.org/10.1029/2019GL083442.

Kollmann, P., Paranicas, C., Clark, G., Roussos, E., Lagg, A., and Krupp, N. (2016), The vertical thickness of Jupiter's Europa gas torus from charged particle measurements, *Geophys. Res. Lett.*, 43, 9425– 9433, doi:10.1002/2016GL070326.

Kollmann, P., et al. (2017), A heavy ion and proton radiation belt inside of Jupiter's rings, Geophys. Res. Lett., 44, 5259– 5268, doi:10.1002/2017GL073730.

Krimigis, S., Mitchell, D., Hamilton, D. et al. A nebula of gases from Io surrounding Jupiter. Nature 415, 994–996 (2002). https://doi.org/10.1038/415994a.

Lagg, A., N. Krupp, J. Woch, and D. J. Williams (2003), In situ observations of a neutral gas torus at Europa, Geophys. Res. Lett., 30(11), 1556, doi:10.1029/2003GL017214.

Mauk, B. H., Williams, D. J., McEntire, R. W., Khurana, K. K., and Roederer, J. G. (1999), Storm-like dynamics of Jupiter's inner and middle magnetosphere, J. Geophys. Res., 104(A10), 22759– 22778, doi:10.1029/1999JA900097.

Mauk, B. H., et al. (2002), Transient aurora on Jupiter from injections of magnetospheric electrons, Nature, 415, 1003-1005, doi:10.1038/4151003a.

Mauk, B. H., D. G. Mitchell, S. M. Krimigis, E. C. Roelof, and C. P. Paranicas (2003), Energetic neutral atoms from a trans-Europa gas torus at Jupiter, Nature, 421, 920, doi:10.1038/nature01431.

Mauk, B. H., Mitchell, D. G., McEntire, R. W., Paranicas, C. P., Roelof, E. C., Williams, D. J., Krimigis, S. M., and Lagg, A. (2004), Energetic ion characteristics and neutral gas interactions in Jupiter's magnetosphere, J. Geophys. Res., 109, A09S12, doi:10.1029/2003JA010270.

Mauk, B. H., Haggerty, D.K., Jaskulek, S.E. et al. (2017), The Jupiter Energetic Particle Detector Instrument (JEDI) Investigation for the Juno Mission. *Space Sci Rev*, 213, Iss. 1-4, pp. 289-346, doi:10.1007/s11214-013-0025-3

Mauk, B. H., Clark, G., Gladstone, G. R., Kotsiaros, S., Adriani, A., Allegrini, F., et al (2020). Energetic Particles and Acceleration Regions over Jupiter's Polar Cap and Main Aurora; a Broad Overview. Journal of Geophysical Research: Space Physics, 125, e2019JA027699. https://doi.org/10.1029/2019JA027699

McComas, D.J., Alexander, N., Allegrini, F. et al. (2017), The Jovian Auroral Distributions Experiment (JADE) on the Juno Mission to Jupiter. *Space Sci Rev*, 213, Iss. 1-4, pp 547-643, doi:10.1007/s11214-013-9990-9.

McEntire, R.W. and Mitchell, D.G. (2013). Instrumentation for Global Magnetospheric Imaging Via Energetic Neutral Atoms. In Solar System Plasma Physics (eds J.H. Waite, J.L. Burch and R.L. Moore). doi:10.1029/GM054p0069

Mitchell, D. G., et al. (2005), Energetic ion acceleration in Saturn's magnetotail: Substorms at Saturn? Geophys. Res. Lett., 32, L20S01, doi:10.1029/2005GL022647.

Mitchell, D. G., Kurth, W. S., Hospodarsky, G. B., Krupp, N., Saur, J., Mauk, B. H., Carbary, J. F., Krimigis, S. M., Dougherty, M. K., and Hamilton, D. C. (2009a), Ion conics and electron

beams associated with auroral processes on Saturn, J. Geophys. Res., 114, A02212, doi:10.1029/2008JA013621.

Mitchell et al. (2009b);, Recurrent energization of plasma in the midnight-to-dawn quadrant of Saturn's magnetosphere, and it relationship ot auroral UV and radio emissions, Planet. And Space Sci, 57, 1732, doi:j.pss.2009.04.22.

Nénon, Q., & André, N. (2019). Evidence of Europa neutral gas torii from energetic sulfur ion measurements. Geophysical Research Letters, 46, 3599– 3606. https://doi.org/10.1029/2019GL082200

Paranicas, C., Mauk, B. H., Haggerty, D. K., Clark, G., Kollmann, P., Rymer, A. M., et al (2019). Io's effect on energetic charged particles as seen in Juno data. Geophysical Research Letters, 46, 13615– 13620. https://doi.org/10.1029/2019GL085393.

Plainaki, C. et al. (2018), Towards a global unified model of Euorpa's tenuous atmosphere, Space Sci. Rev., 214:40, https://doi.org/10.1007/s11214-018-0469-6.

Roelof, E. C. (1987), Energetic neutral atom image of a storm-time ring current, J. Geophys. Res., 14, 6, 652-655, doi.org/10.1029/GL014i006p00652.

Smith, T. D., D. G. Mitchell, R. E. Johnson, B. H. Mauk, and J. E. Smith (2019), Europa neutral torus confirmation and characterization based on observations and modeling, The Astrophysical Journal, 871:69, https://doi.org/10.3847/1538-4357/aaed38.

Smyth, S. H. and M. L. Marconi (2006), Euorpa's atmosphere, gas tori, and magnetospheric implications, Ecarus, 181(2), 510, https://doi.org/10.1016/j.icarus.2005.10.019.

Szalay, J. R., et al. (2017), Plasma measurements in the Jovian polar region with Juno/JADE. *Geophys. Res. Lett.*, 44, 7122– 7130, doi:10.1002/2017GL072837.

Thorne, R. M., T. P. Armstrong S. Stone D. J. Williams R. W. McEntire S. J. Bolton D. A. Gurnett M. G. Kivelson (1997), Galileo evidence for rapid interchange transport in the Io torus, Geophys. Res. Lett., 24, 17, 2134, doi:10.1029/97GL01788.

Figure 1. (a) Schematic of the configuration of Juno's trajectory close to Jupiter during the perijove number 22 (PJ22) plotted within the XZ plane in the Jupiter Sun Orbit (JSO) coordinated system. (b) Configuration of the three sensors (J90, J180, J270) that comprise the Jupiter Energetic particle Detector Instrument (JEDI). This figure also defines the angle called "Azimuth". See the text for further details of both (a) and (b).

Figure 2. Various displays of the JEDI Oxygen (O) plus Sulfur (S) channels for the outbound leg of the Juno perijove 22. (Panel 1) Intensity versus pitch angle distributions as a function of time averaged over 30 second intervals. (Panel 2) Intensity versus azimuth distributions plotted as a function of time for the same data, averaged over 300 second intervals. Figure 1b defines Azimuth. (Panel 3) Counts-per-bin versus azimuth distributions plotted as a function of time, averaged over 600 second intervals. (Panel 4) Intensity versus energy distributions plotted as a function of time for O+S measurements with pitch angles greater than 110°, averaged over 600 second intervals. That selection of pitch angles results in the exclusion of some of the ions and preferentially selects ENA data. Because the averaging process includes a lot of empty space, the Intensity scale for this panel has been renormalized so that the lowest energy channel has an

intensity that matches that channel's intensity for the most prominent ENA feature. In panels 2 and 3, various features are named in the left portions of the panels, as described in the text. The dipole component of the JRM09 magnetic field model (Connerney et al., 2018) are used to derived the magnetic latitudes and L-values on the time scale.

Figure 3. Quantification of the 3 features identified in Figure 2. (a) This panel has averaged azimuth centroids of the 3 features as a function of time. The lines overlaying the scatter plots are analytic fits, with the equations for the fits given in the text. These fits are used in subsequent analyses to determine the JEDI viewing as a function of time relative to the Jovian system. (b) Total counts within each feature as a function of time. The error bars are ±1 standard deviations ($\sqrt{N}$) for the average counts within each feature (Average counts are: A:17.0; B:11.7; C:6.6). For both panels, the averaging interval is 600 seconds, with a cadence of 300 seconds.

Figure 4. Various displays of the JEDI Hydrogen channels for the outbound leg of the Juno perijove 22. Except for the change in mass species, the caption to Figure 2 describes the panels.

Figure 5. Analysis of the viewing of JEDI that yields the three different structures in Figures 2 and 3, shown within the JSO YZ plane. Green lines, grey lines, and dashed blue lines show the viewings for Features A, B, and C, respectively. The small red and blue circles show the positions of the orbits of Io and Europa, respectively.

Figure 6. Same as Figure 3a but augmented with an analysis showing what kinds of shifts are needed to alter the interpretations of the features. The shifts for Features A, B, and C are 9.5°, 9°, and 12°, respectively. See the text for more information.

Figure 7. Same as Figure 5 but here shown in the JSO XZ plane (a) and the JSO XY plane (b). In panel (b), dashed red and blue arrows show the positions of Io and Europa, respectively, within their orbits at 0500 and 0800. Also shown in (b) is the approximate position where Juno crossed the L-shell of Io on its inbound leg.

Figure 8. Various displays of the JEDI Oxygen (O) plus Sulfur (S) channels for the outbound leg of the Juno perijove 23. The Figue 2 caption describes the panels.

Figure 9. JEDI electron and ion channels data from the inbound leg of Juno perijove 22. (Panel 1) Intensity versus time of selected JEDI O+S ion channels. The red-dashed line is an estimate of the electron-induced noise in the 145-209 keV channel. (Panel 2) Proton Intensity versus energy plotted as a function of time. (Panel 3) Electron intensity versus energy plotted as a function of time. The energy scale is inverted for this panel. (Panel 4) Electron basic rates from special solid state detectors (SSDs) in the JEDI unit J180. Here telescopes T1 and T3 have a shield in front of them, whereas telescopes T2, T4, and T5 are bare. When these 5 measurements pinch together on the right-hand-portion of the plot, that means that the electron measurements in Panels 3 and 4 are dominated by very high-energy electrons that penetrate the side box of the instrument. The dipole component of the JRM09 magnetic field model (Connerney et al., 2018) are used to derived the magnetic latitudes and L-values on the time scale.

Figure 10. JEDI electron and ion channels data from the inbound leg of Juno perijove 23. The caption to Figure 8 describes the panels.

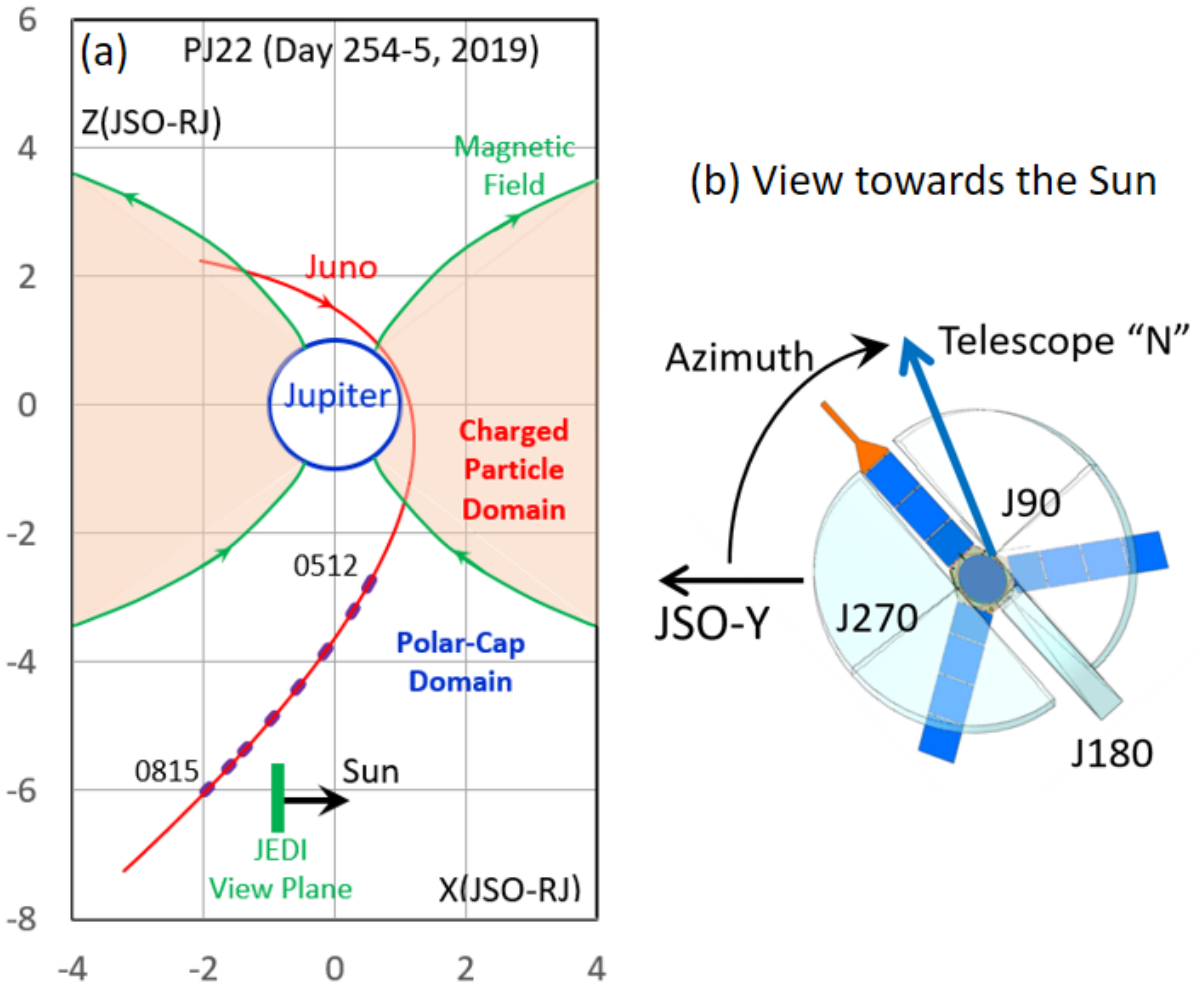
(a) PJ22 (Day 254-5, 2019)
Z(JSO-RJ)
Magnetic Field
Juno
Jupiter
Charged Particle Domain
0512
Polar-Cap Domain
0815
Sun
JEDI View Plane
X(JSO-RJ)
6
4
2
0
-2
-4
-6
-8
-4
-2
0
2
4
(b) View towards the Sun
Azimuth
Telescope "N"
JSO-Y
J90
J270
J180

Figure 1

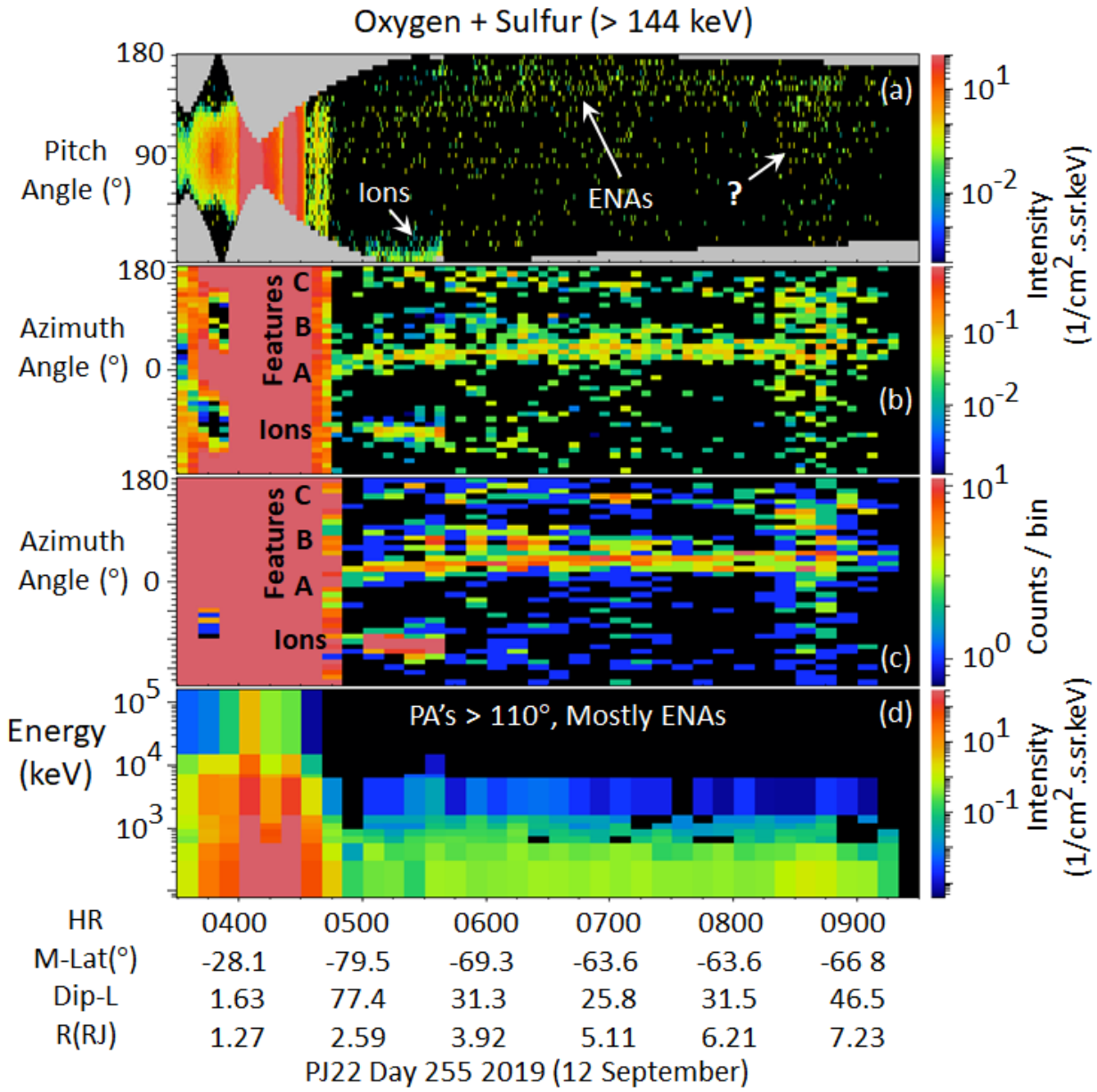
Oxygen + Sulfur (> 144 keV)
Pitch Angle (°)
180
90
Ions
ENAs
?
(a)
Azimuth Angle (°)
0
Features
C
B
A
Ions
(b)
(c)
Intensity (1/cm^2.s.sr.keV)
Counts / bin
Energy (keV)
10^5
10^4
10^3
PA's > 110°, Mostly ENAs
(d)
HR 0400 0500 0600 0700 0800 0900
M-Lat(°) -28.1 -79.5 -69.3 -63.6 -63.6 -66 8
Dip-L 1.63 77.4 31.3 25.8 31.5 46.5
R(RJ) 1.27 2.59 3.92 5.11 6.21 7.23
PJ22 Day 255 2019 (12 September)

Figure 2

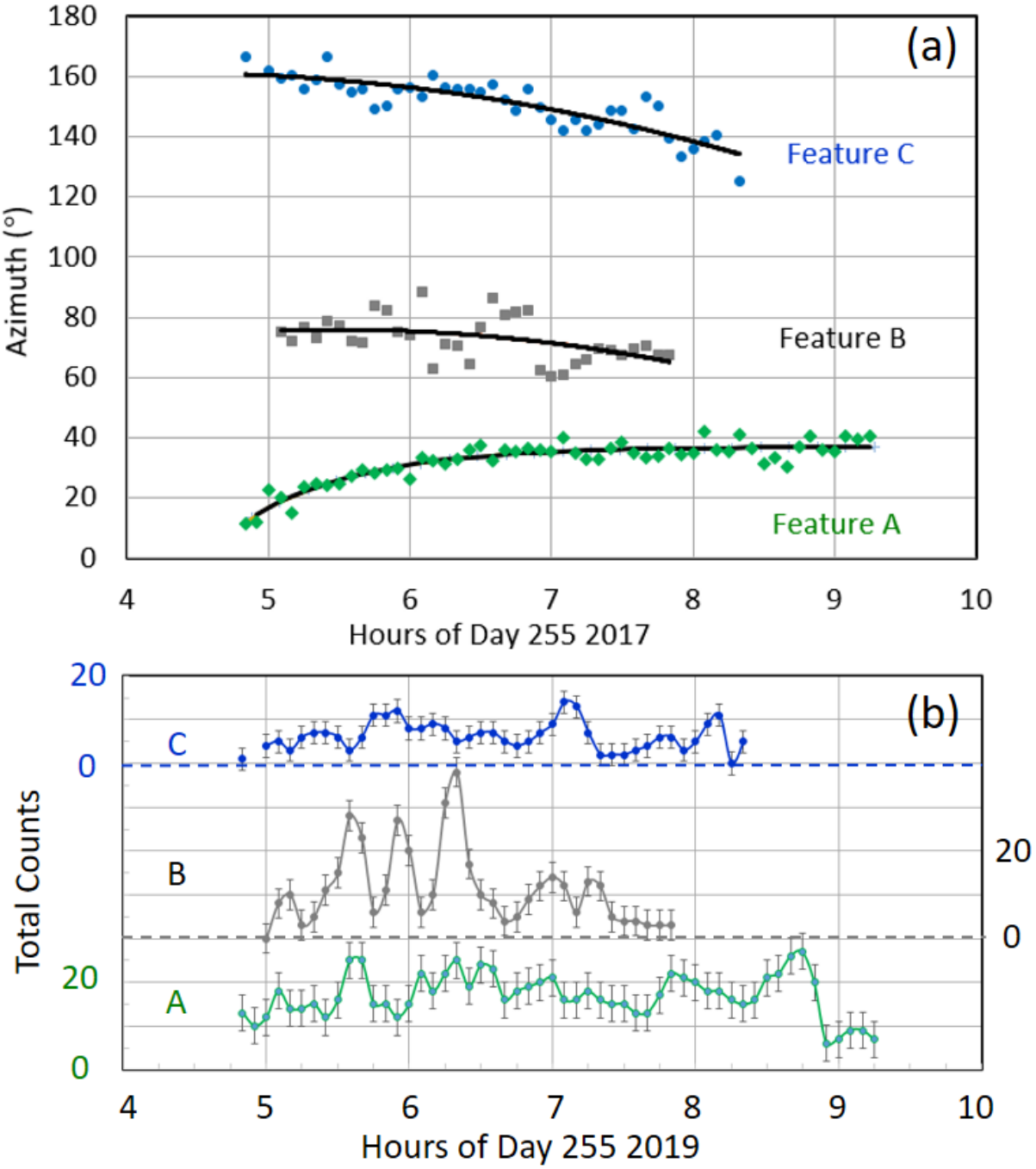
(a)
Azimuth (°)
180
160
140
120
100
80
60
40
20
0
Feature C
Feature B
Feature A
4
5
6
7
8
9
10
Hours of Day 255 2017
(b)
Total Counts
20
0
C
B
20
0
A
20
0
4
5
6
7
8
9
10
Hours of Day 255 2019

Figure 3

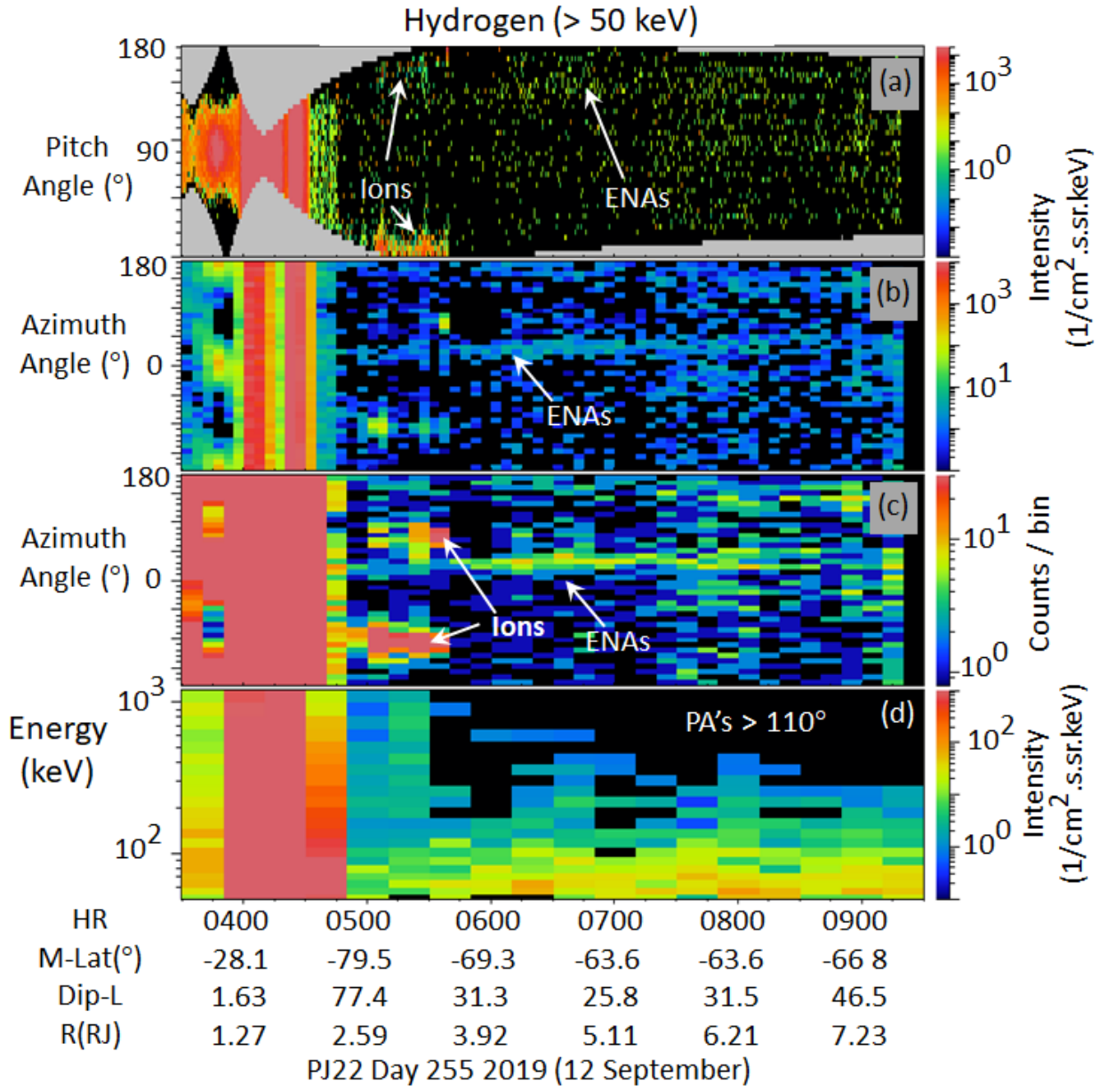
Hydrogen (> 50 keV)
180
Pitch
Angle (°)
90
Ions
ENAs
(a)
10^3
10^0
Intensity
(1/cm^2.s.sr.keV)
180
Azimuth
Angle (°)
0
ENAs
(b)
10^3
10^1
180
Azimuth
Angle (°)
0
Ions
ENAs
(c)
10^1
10^0
Counts / bin
10^3
Energy
(keV)
10^2
PA's > 110°
(d)
10^2
10^0
Intensity
(1/cm^2.s.sr.keV)
HR 0400 0500 0600 0700 0800 0900
M-Lat(°) -28.1 -79.5 -69.3 -63.6 -63.6 -66 8
Dip-L 1.63 77.4 31.3 25.8 31.5 46.5
R(RJ) 1.27 2.59 3.92 5.11 6.21 7.23
PJ22 Day 255 2019 (12 September)

Figure 4

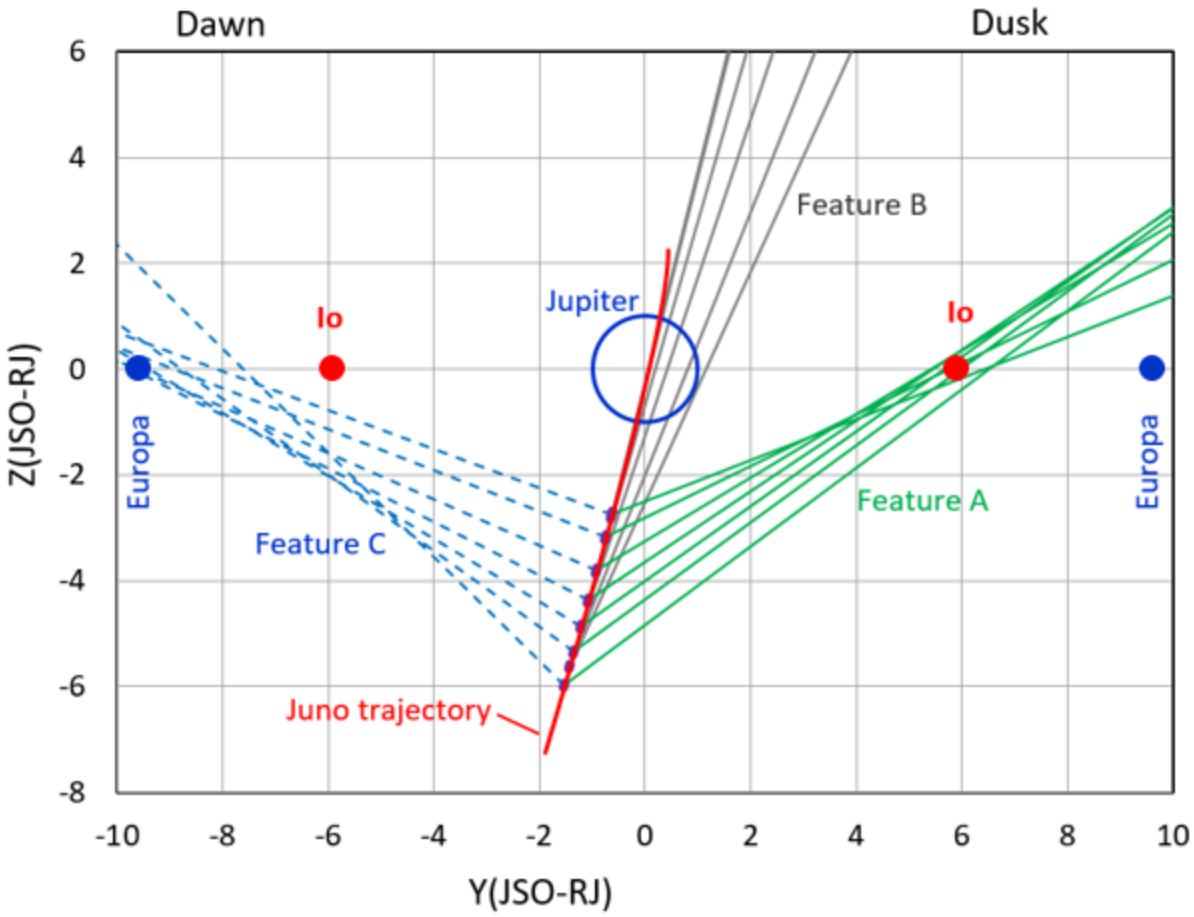
Dawn
Dusk
Feature B
Jupiter
Io
Io
Europa
Europa
Feature A
Feature C
Juno trajectory
Z(JSO-RJ)
Y(JSO-RJ)
6
4
2
0
-2
-4
-6
-8
-10
-8
-6
-4
-2
0
2
4
6
8
10

Figure 5

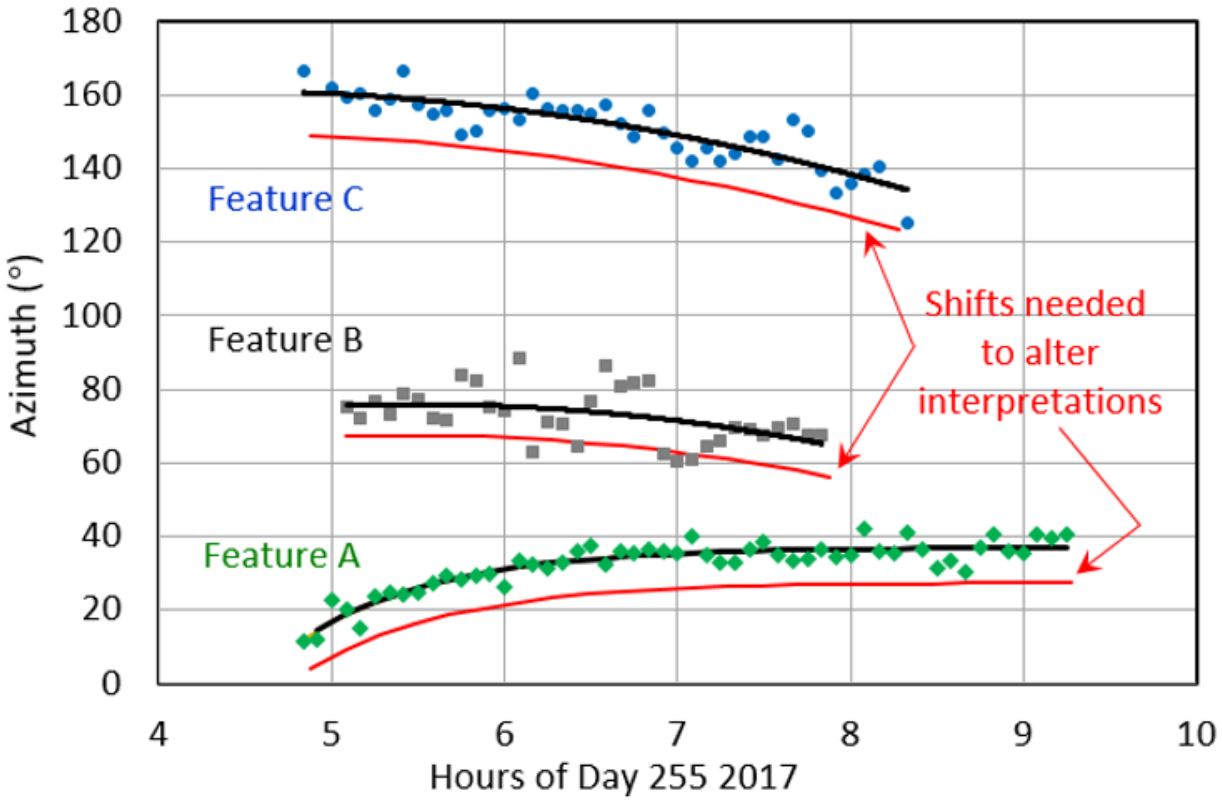
180
160
140
120
100
80
60
40
20
0
Azimuth (°)
Feature C
Feature B
Feature A
Shifts needed
to alter
interpretations
4
5
6
7
8
9
10
Hours of Day 255 2017

Figure 6

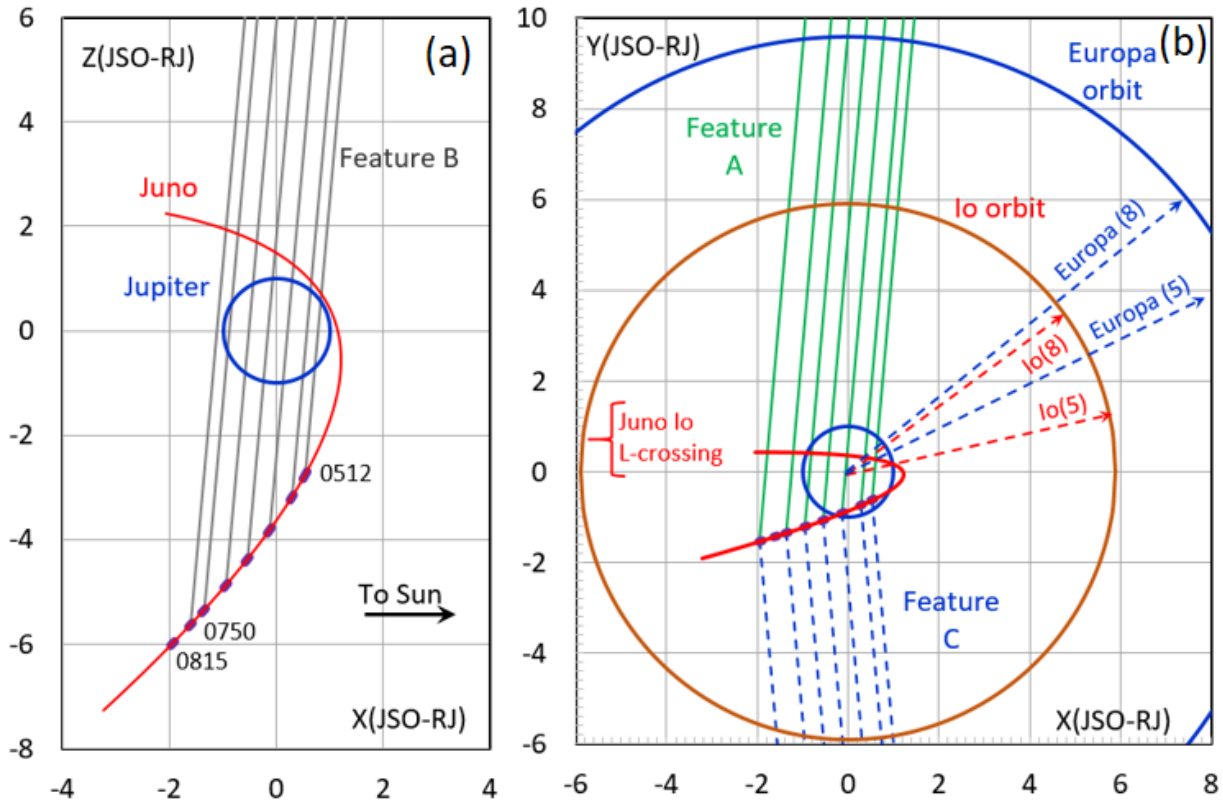
Z(JSO-RJ)
(a)
Feature B
Juno
Jupiter
0512
0750
0815
To Sun
X(JSO-RJ)
Y(JSO-RJ)
Europa orbit
(b)
Feature A
Io orbit
Europa (8)
Europa (5)
Io(8)
Io(5)
Juno Io L-crossing
Feature C
X(JSO-RJ)

Figure 7

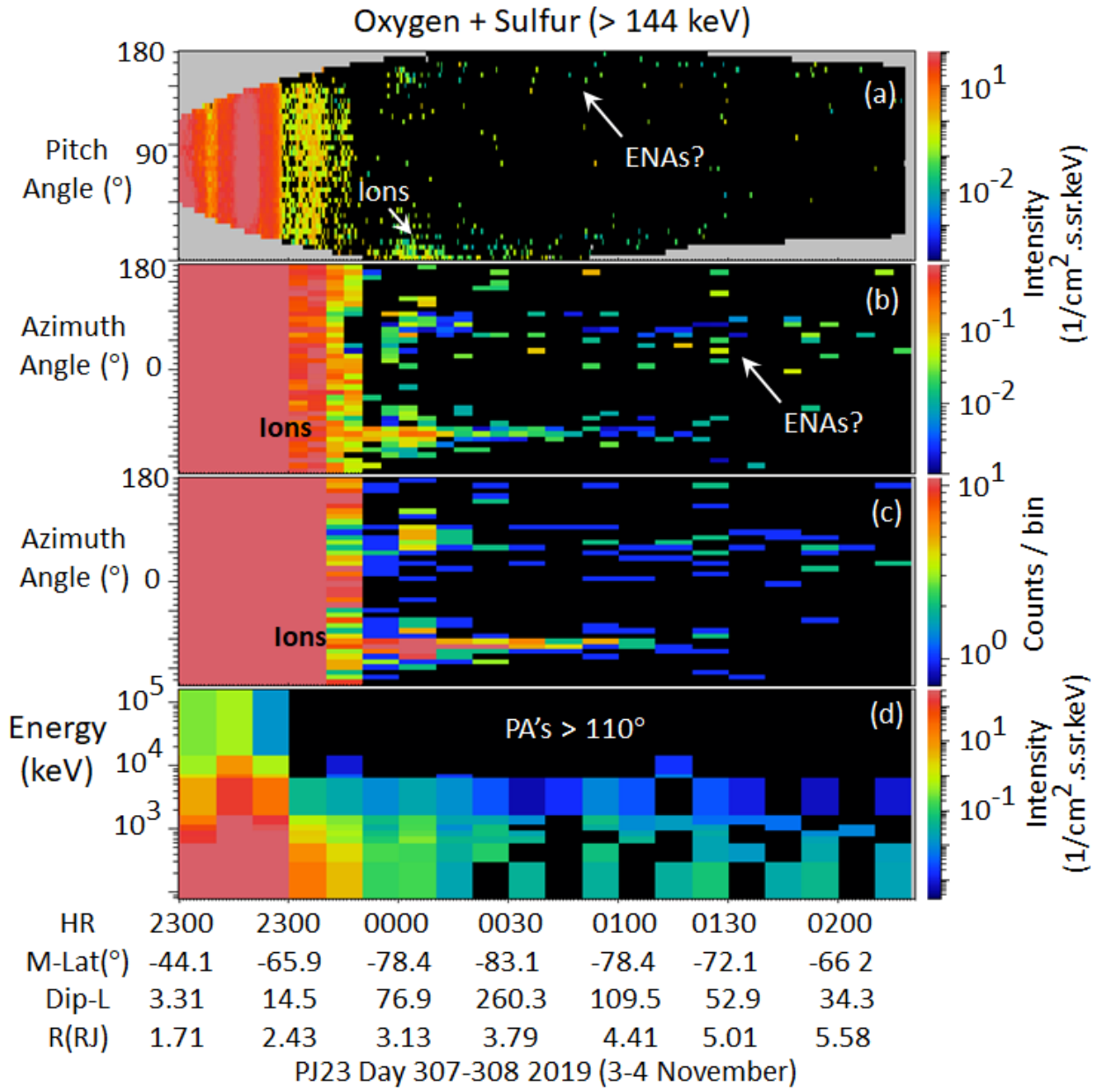
Oxygen + Sulfur (> 144 keV)
Pitch Angle (°)
180
90
(a)
ENAs?
Ions
Intensity (1/cm².s.sr.keV)
Azimuth Angle (°)
0
(b)
Ions
ENAs?
(c)
Counts / bin
Energy (keV)
(d)
PA's > 110°
HR 2300 2300 0000 0030 0100 0130 0200
M-Lat(°) -44.1 -65.9 -78.4 -83.1 -78.4 -72.1 -66 2
Dip-L 3.31 14.5 76.9 260.3 109.5 52.9 34.3
R(RJ) 1.71 2.43 3.13 3.79 4.41 5.01 5.58
PJ23 Day 307-308 2019 (3-4 November)

Figure 8

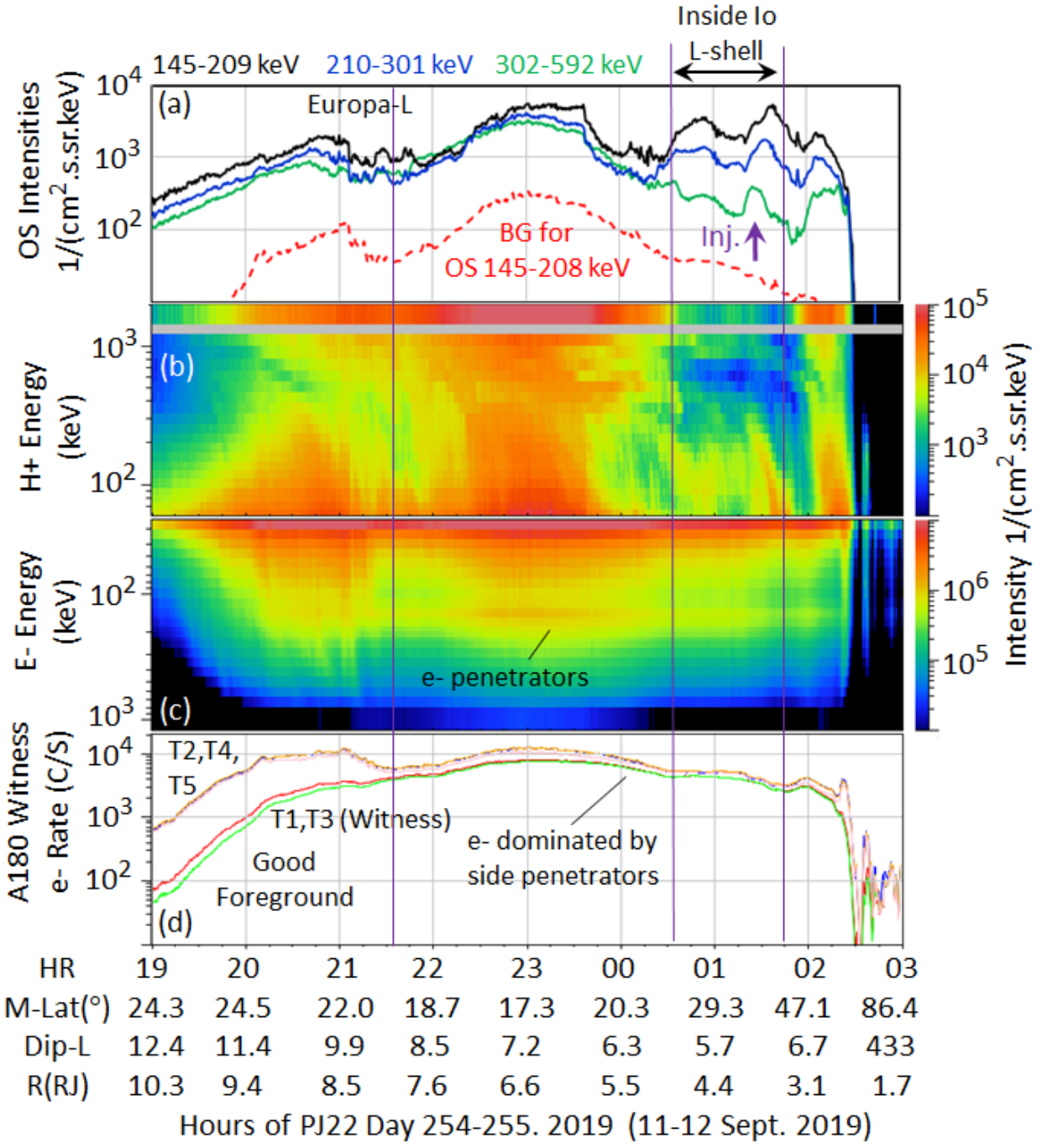
Inside Io
L-shell
145-209 keV
210-301 keV
302-592 keV
OS Intensities 1/(cm2.s.sr.keV)
(a)
Europa-L
BG for
OS 145-208 keV
Inj.
H+ Energy (keV)
(b)
E- Energy (keV)
e- penetrators
(c)
Intensity 1/(cm2.s.sr.keV)
A180 Witness e- Rate (C/S)
T2,T4,
T5
T1,T3 (Witness)
Good
Foreground
e- dominated by
side penetrators
(d)
HR 19 20 21 22 23 00 01 02 03
M-Lat(°) 24.3 24.5 22.0 18.7 17.3 20.3 29.3 47.1 86.4
Dip-L 12.4 11.4 9.9 8.5 7.2 6.3 5.7 6.7 433
R(RJ) 10.3 9.4 8.5 7.6 6.6 5.5 4.4 3.1 1.7
Hours of PJ22 Day 254-255. 2019 (11-12 Sept. 2019)

Figure 9

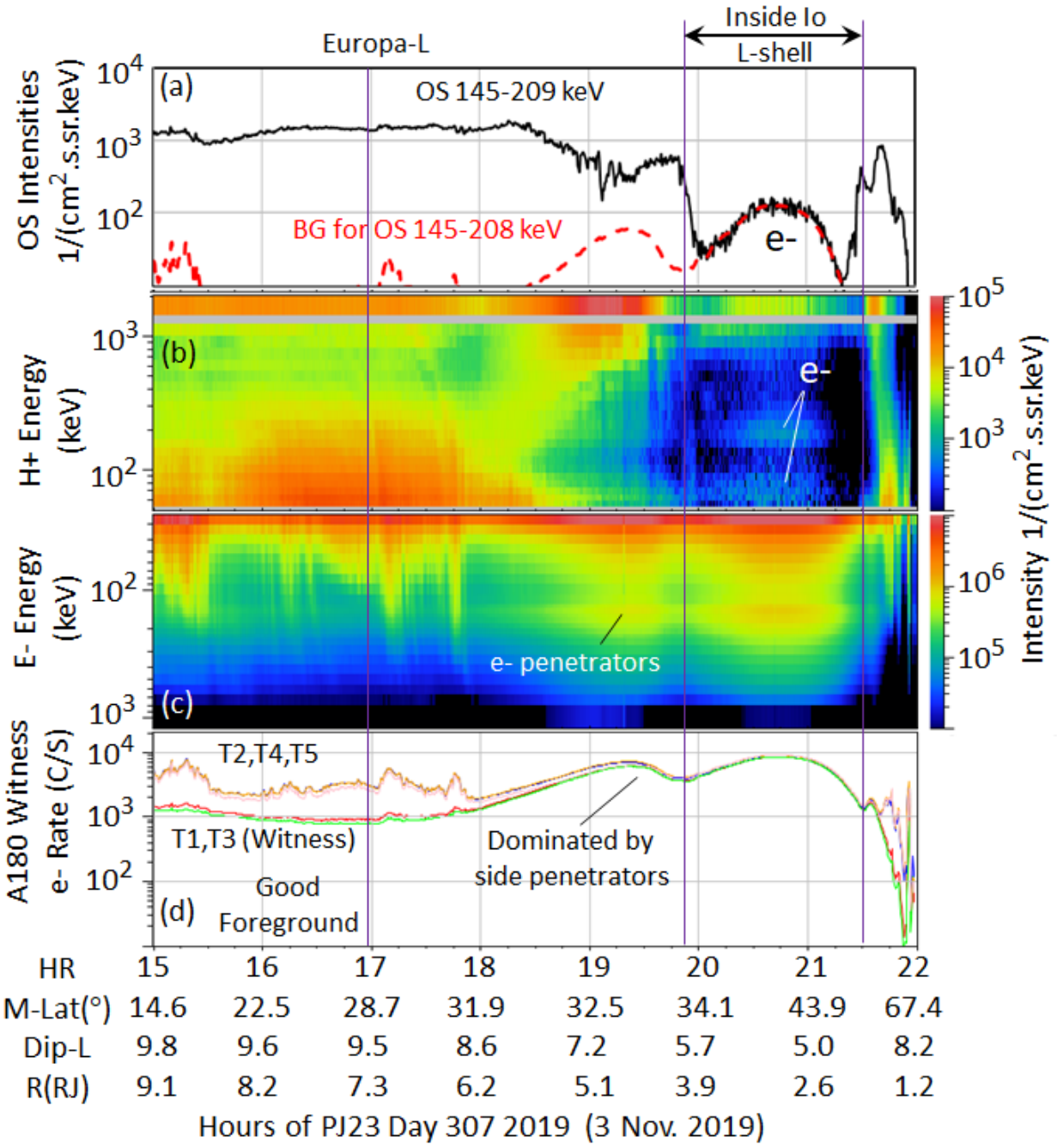
Inside Io
L-shell
Europa-L
OS Intensities
1/(cm2.s.sr.keV)
(a)
OS 145-209 keV
BG for OS 145-208 keV
e-
H+ Energy
(keV)
(b)
e-
E- Energy
(keV)
e- penetrators
(c)
Intensity 1/(cm2.s.sr.keV)
A180 Witness
e- Rate (C/S)
T2,T4,T5
T1,T3 (Witness)
Dominated by
side penetrators
Good
Foreground
(d)
HR 15 16 17 18 19 20 21 22
M-Lat(°) 14.6 22.5 28.7 31.9 32.5 34.1 43.9 67.4
Dip-L 9.8 9.6 9.5 8.6 7.2 5.7 5.0 8.2
R(RJ) 9.1 8.2 7.3 6.2 5.1 3.9 2.6 1.2
Hours of PJ23 Day 307 2019 (3 Nov. 2019)

Figure 10